IOP Conf. Series: Materials Science and Engineering **724** (2020) 012024 doi:10.1088/1757-899X/724/1/012024

Theoretical Analysis of Spherical Bearings Lubricated with Greases

A V Radulescu[1], I Radulescu[1]

[1]University POLITEHNICA Bucharest, Romania

E-mail: alexandru.radulescu@upb.ro

Abstract. The paper presents theoretical researches concerning the spherical bearings lubricated with greases, in rheostatic conditions: high loads and low velocities. This type of bearing is very appropriate for modelling the human joints (hip, knee), spherical joints from automotive industry (pivots, connecting rods) or special joints from petroleum industry. Spherical bearings may be of the "fitted" type or the "clearance" type. The fitted type of nonflat bearing pad surface is lapped-in to fit the runner. When it is operating, the fitted pad will have a varying film thickness across the pad sill, between the pad and the runner. Similarly, in the clearance type the film shape will be non-uniform across the pad sill. The variation in film thickness across the bearing pad, for nonflat pads, influences the resulting pressure distribution in the bearing pad and, hence, its load carrying capacity. In this paper, the pressure distribution and the load capacity are determined for „clearance" type bearings, for two different cases: complete spherical bearings and partial spherical bearings. It has been found that the eccentricity ratio influences the angular position of the maximum pressure, which becomes nearer to the minimum angle of the bearing, once with the increasing of the eccentricity ratio.

NOMENCLATURE

$C_F = \bar{F}\psi$	Load coefficient	y	Cartesian coordinate
D	Spherical pad diameter	$\epsilon = 2e/J$	Eccentricity ratio
F	Load carrying capacity	η	Viscosity
$\bar{F} = \frac{F}{\pi D^2 \tau_0}$	Non-dimensional load carrying capacity	θ	Angular coordinate
J	Clearance	θ^*	Angle corresponding to the maximum pressure
d	Spherical ball diameter	θ_{max}	Maximum angle of the spherical bearing
e	Eccentricity	θ_{min}	Minimum angle of the spherical bearing
h	Film thickness	τ	Shear stress
p	Pressure	τ_0	Yield stress
$\bar{p} = p/p_{max}$	Non-dimensional pressure	$(\tau:\tau)/2$	Second invariant of the tangential stress tensor
u	Velocity	$\psi = J/D$	Relative clearance

1. Introduction

The classical hydrodynamic lubrication theory in its original form can be applied only if the lubricant behaves as a linearly viscous fluid (Newtonian). Applications involving non-Newtonian fluids require appropriate formulation [1]. A class of non-Newtonian fluid utilizes a so-called Bingham model in some tribological applications to describe the flow characteristics of some lubricants, such as grease or fine suspensions [2]. Two parameters, which characterize Bingham plastic models, are the yield stress and the viscosity. When the magnitude of the stress tensor is less than the yield stress, the behaviour of the fluid is akin to that of a rigid solid. When the yield stress is exceeded, an ideal Bingham plastic fluid commences to flow as a linear viscous (Newtonian) liquid [3].

The purpose of this paper is to study the spherical bearings lubricated with greases, in rheostatic conditions: high loads and low velocities. This type of bearing is very appropriate for modelling the human joints, such as the synovial joint (Figure 1) [4 - 7] or the spherical joints used in the motor vehicle industry, such as pivots and auxiliary connecting rods (Figure 2) [8 - 10].

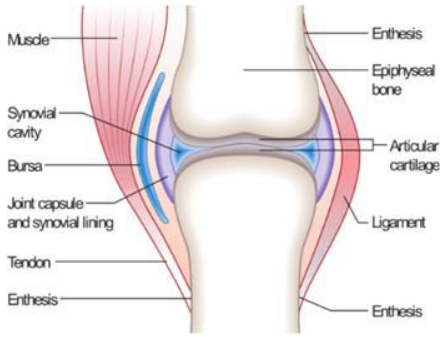

Figure 1. Human synovial joint [4]

Figure 2. Spherical joints from motor vehicle industry [8]

2. Theory

Special nonflat bearings pad can handle unusual load and motion requirements that flat thrust pads cannot. For instance, spherical-pad bearings are free to rotate about the three major axes without disrupting operation of the bearing. Spherical bearings may be of the "fitted" type or the "clearance" type [11 – 12]. The fitted type of nonflat bearing pad surface is lapped-in to fit the runner. When in operation, the fitted pad will have a varying film thickness across the pad sill between the pad and the runner. Similarly, in the clearance type the film shape will be nonuniform across the pad sill. An exception to this is when the combination of load and flow is such as to cause the bearing to operate in the "concentric" position. The variation in film thickness across the bearing pad for nonflat pads influences the resulting pressure distribution in the bearing pad and, hence, its load carrying capacity.
In this paper, only the clearance bearings are considered, for two different cases: complete spherical bearings and partial spherical bearings. The geometry of these bearings is presented in Figure 3 and Figure 4.

In these cases, the spherical pad radius is slightly larger than the spherical ball radius and the film thickness between the pad sill and the ball will vary with the angular coordinate such that:

$$h = \frac{J}{2} - e\cos\theta \tag{1}$$

The rheological model for the non-Newtonian fluid is ideal Bingham plastic model. The constitutive equation for the fluid is:

$$\tau = \tau_0 + \eta\frac{du}{dy} \tag{2}$$

For the general case of Bingham fluid, Oldroyd propose a three-dimensional rheostatic equation, based on the Mises plasticity criterion [13 - 14]:

$$\left|\frac{1}{2}(\tau:\tau)\right| \leq \tau_0^2 \tag{3}$$

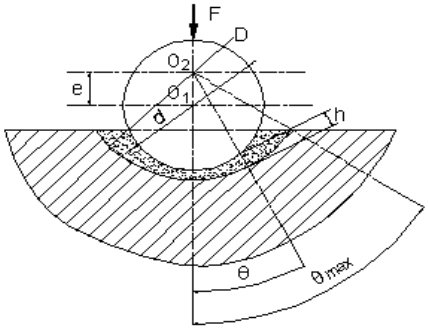

Figure 3. Complete spherical bearing

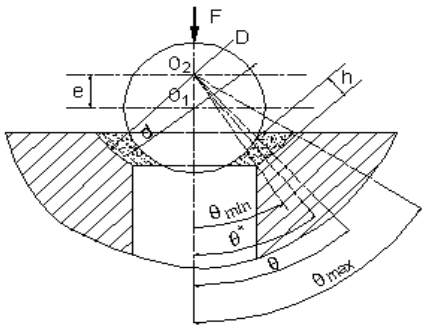

Figure 4. Partial spherical bearing

Due to the fact that the spherical bearings considered in Figures 3 and 4 are symmetrical, equation (3) becomes simpler and can be treated analytically [15]. Taking account that the lubricant flow is circumferential, the rheostatic equation for the spherical bearings will be:

$$\frac{dp}{d\theta} = -\frac{D\tau_0}{h} \tag{4}$$

The pressure distribution can be obtained integrating equation (4) and considering the film thickness given by the equation (1):

$$p(\theta) = \int \left(-\frac{D\tau_0}{\frac{J}{2} - e\cos\theta} \right) d\theta \tag{5}$$

If the surface of the spherical bearing is noted with Ω and $\Gamma = \bigcup_{i=1}^{n} \Gamma_i$ represent the curves adjacent to the surface Ω, the limit conditions for the pressure distribution (5) are:

$$p|_{(x,y)\in\bigcup_{i=1}^{n}\Gamma_i} = 0 \tag{6}$$

For this case, the load carrying capacity of the bearing is calculated by integrating the pressure distribution obtained from equation (5):

$$F = \int_{\Omega} p d\Omega \tag{7}$$

2.1 Complete spherical bearing

Considering the geometry of the complete spherical bearing (see Figure 3) and imposing the limit condition:

$$p = 0 \quad \text{for} \quad \theta = \theta_{max} \tag{8},$$

the pressure distribution results by integrating the equation (5):

$$p = \frac{4D\tau_0}{\sqrt{J^2-4e^2}} \left[arctg \frac{(J+2e)tg\frac{\theta_{max}}{2}}{\sqrt{J^2-4e^2}} - arctg \frac{(J+2e)tg\frac{\theta}{2}}{\sqrt{J^2-4e^2}} \right] \tag{9}$$

In order to obtain the load carrying capacity (eq. 7), the pressure distribution must be integrated:

$$F = \frac{\pi D^2}{2} \int_0^{\theta_{max}} p \sin\theta \cos\theta \, d\theta \tag{10}$$

Unfortunately, no analytical solution can be obtained and a numerical solution is imposed.
Therefore, the following non-dimensional notations are necessary:

$$\varepsilon = \frac{2e}{J}; \quad \psi = \frac{J}{D}; \quad \bar{p} = \frac{p}{p_{max}}; \quad \bar{F} = \frac{F}{\pi D^2 \tau_0}; \quad C_F = \bar{F}\psi \tag{11}$$

2.2 Partial spherical bearing

The case of the partial spherical bearing (Figure 4) is treated similar to the case of the complete spherical bearings, excepting the limit conditions for the pressure distribution. These conditions must be imposed on two adjacent curves of the surface Ω, corresponding to the maximum and minimum angles of the spherical bearing:

$$p = 0 \quad \text{for} \quad \theta = \theta_{max} \qquad \text{and} \qquad p = 0 \quad \text{for} \quad \theta = \theta_{min} \tag{12}$$

Integrating the equation (5), the pressure distribution is obtained for two different zones:

$$p = \begin{cases} \frac{4D\tau_0}{\sqrt{J^2-4e^2}}\left[arctg\frac{(J+2e)tg\frac{\theta}{2}}{\sqrt{J^2-4e^2}} - arctg\frac{(J+2e)tg\frac{\theta_{min}}{2}}{\sqrt{J^2-4e^2}}\right] & \text{for } \theta \in [\theta_{min};\theta^*] \\ \frac{4D\tau_0}{\sqrt{J^2-4e^2}}\left[arctg\frac{(J+2e)tg\frac{\theta_{max}}{2}}{\sqrt{J^2-4e^2}} - arctg\frac{(J+2e)tg\frac{\theta}{2}}{\sqrt{J^2-4e^2}}\right] & \text{for } \theta \in (\theta^*;\theta_{max}] \end{cases} \quad (13),$$

where θ^*represents the angle corresponding to the maximum pressure. This value is obtained by solving numerically the following equation and using the non-dimensional notations (11):

$$arctg\frac{(1+\varepsilon)tg\frac{\theta^*}{2}}{\sqrt{1-\varepsilon^2}} = \frac{1}{2}\left[arctg\frac{(1+\varepsilon)tg\frac{\theta_{max}}{2}}{\sqrt{1-\varepsilon^2}} + arctg\frac{(1+\varepsilon)tg\frac{\theta_{min}}{2}}{\sqrt{1-\varepsilon^2}}\right] \quad (14)$$

Finally, the load carrying capacity is numerically obtained by integrating the pressure distribution (eq. 13) from minimum angle of the spherical bearing to the maximum angle:

$$F = \frac{\pi D^2}{2}\int_{\theta_{min}}^{\theta_{max}} p\,sin\,\theta\,cos\,\theta\,d\theta \quad (15)$$

3. Results

3.1 Complete spherical bearing

Figure 5 shows the spatial distribution of the non-dimensional pressure for four different maximum angles of the complete spherical bearing, in the case when the eccentricity ratio is $\varepsilon = 0.9$.

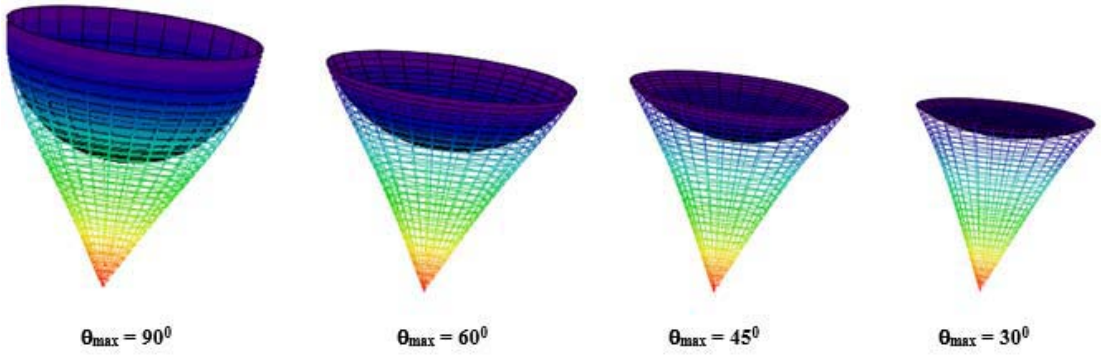

Figure 5. Spatial distribution of the non-dimensional pressure (ε = 0.9)

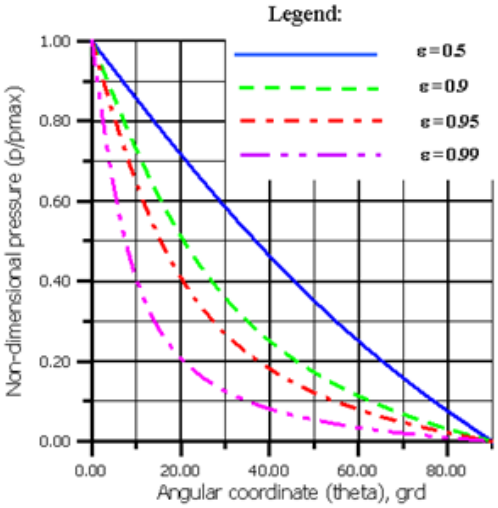

Figure 6. Pressure distribution (cross section $\theta_{max} = 90^0$)

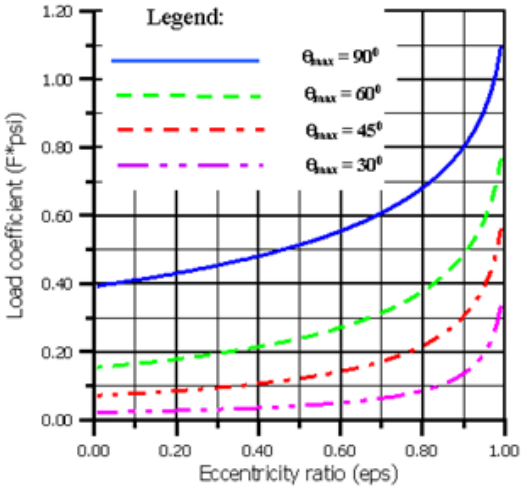

Figure 7. Variation of the load coefficient

Also, Figure 6 presents a cross section through the spatial distribution of the non-dimensional pressure, in order to study the influence of the eccentricity ratio on the pressure profile. Figure 7 presents the variation of the load coefficient versus eccentricity ratio for different values of the maximum angle of the complete spherical bearing.

3.2 Partial spherical bearing

Figure 8 shows the spatial distribution of the non-dimensional pressure for the eccentricity ratio $\varepsilon = 0.9$ and Figure 9 shows the same pressure distribution in the cross section for different values of minimum and maximum angles of the partial spherical bearing. Also, Figure 10 presents the position of the angle corresponding to the maximum pressure versus eccentricity ratio, for the same values of angles.

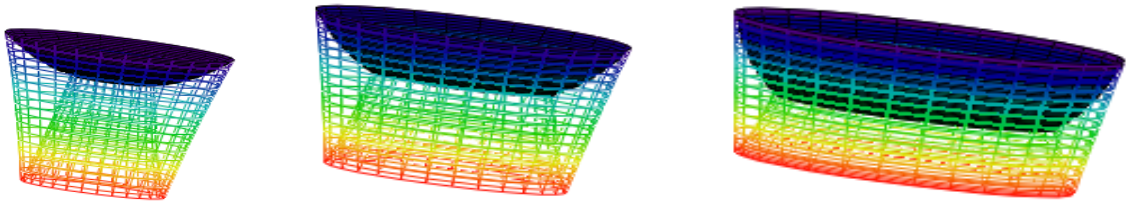

$\theta_{min} = 15^0$ $\theta_{min} = 30^0$ $\theta_{min} = 45^0$

Figure 8. Spatial distribution of the non-dimensional pressure (ε = 0.9)

The variation of the load coefficient versus the eccentricity ratio for different values of minimum and maximum angle of the partial spherical bearing is presented in Figure 11.

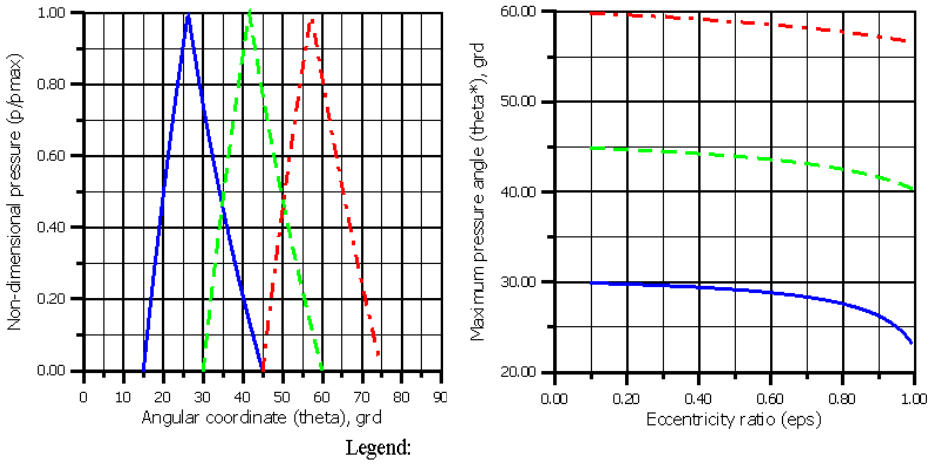

Figure 9. Pressure distribution

Figure 10. Maximum pressure angle

4. Conclusions

1. The influence of the eccentricity ratio on the profile of the pressure distribution is very important for the complete spherical bearing.
2. The load carrying capacity for the complete spherical bearing increases with the increasing of the eccentricity ratio and the maximum angle of the spherical bearing.
3. In the case of the partial spherical bearing, the influence of the eccentricity ratio on the pressure distribution is practically negligible. It has been found that the eccentricity ratio influences

especially the angular position of the maximum pressure, which becomes nearer to the minimum angle of the bearing once with the increasing of the eccentricity ratio

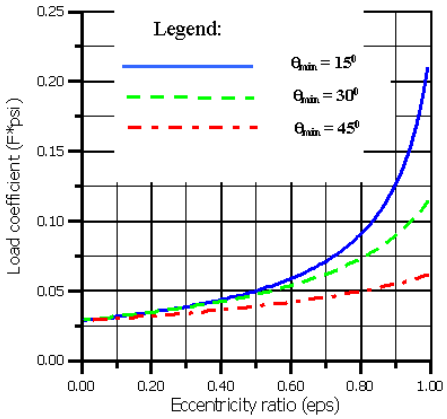

Figure 11. Variation of the load coefficient

4. For the partial spherical bearing, the load carrying capacity also increases with the increasing of the eccentricity ratio and with the decreasing of the minimum angle of the spherical bearing.

5. References

[1] C Balan 2000 *The rheology of lubricating grease* (Amsterdam: ELGI)
[2] T Mang and W Dresel 2007 *Lubricants and Lubrication* (Weinheim: Wiley-Vch)
[3] P M Lugt 2009 A review on grease lubrication in rolling bearings *Tribol. Trans.* **52** (4) pp 470-480
[4] *** https://www.pdhpe.net/the-body-in-motion/how-do-the-musculoskeletal-and-cardiorespiratory-systems-of-the-body-influence-and-respond-to-movement/skeletal-system/structure-function-synovial-joints/ (accessed on 11.04.2019)
[5] M Daniel, A Iglic and V Kralj-Iglic 2005 The shape of acetabular cartilage optimizes hip contact stress distribution *J. Anat.* **207** (1) pp 85-91
[6] M A Wimmer, G Sibylle, T Kaup, M Hänni, E Schneider, S Gogolewski and M Alini 2004 Tribology approach to the engineering and study of articular cartilage *Tissue Eng.* **10** (9-10) pp 1436-1445
[7] M Kothari, J F Booker and D L Bartel 1995 Analysis of artificial hip joints as spherical bearings *Proc. 21th Leeds-Lyon Symposium on Tribology (Leeds)* (Amsterdam: Elsevier) pp 93-98
[8] *** https://en.wikipedia.org/wiki/Ball_joint
[9] M M Khonsari and E R Booser 2017 *Applied tribology: bearing design and lubrication* (New York: John Wiley & Sons)
[10] M J Neale 2013 *Bearings: a tribology handbook* (Amsterdam: Elsevier)
[11] A Harnoy 2002 *Bearing design in machinery: engineering tribology and lubrication* (New York: CRC Press)
[12] B W Rowe 2012 *Hydrostatic, aerostatic and hybrid bearing design* (Amsterdam: Elsevier)
[13] J M Piau 1996 Flow of a yield stress fluid in a long domain. Application to flow on an inclined plane *J. Rheol.* **40** (4) pp 711-723
[14] R Mas and A Magnin 1996 Rheological and physical studies of lubricating greases before and after use in bearings *J. Tribol.* **118** (3) pp 681-686
[15] M D Pascovici and A V Radulescu 1984 Portanta statica a filmului de unsoare consistenta *Proc. Int. Conf. TRIBOTEHNICA '84 (Iasi)* vol 1 pp 295-302